Magnetic diffusion, inductive shielding, and the Laplace transform

Alexander E. Krosney, Michael Lang, Jakob J. Weirathmueller, and Christopher P. Bidinosti

---

ARTICLES YOU MAY BE INTERESTED IN

Schrödinger's equation as a diffusion equation
American Journal of Physics **89**, 500 (2021); https://doi.org/10.1119/10.0002765

Space-time computation and visualization of the electromagnetic fields and potentials generated by moving point charges
American Journal of Physics **89**, 482 (2021); https://doi.org/10.1119/10.0003207

Particle velocity = group velocity: A common assumption in the different theories of Louis de Broglie and Erwin Schrödinger
American Journal of Physics **89**, 521 (2021); https://doi.org/10.1119/10.0003165

Simple derivation of the explicit forms of quantum-mechanical fundamental representations
American Journal of Physics **89**, 535 (2021); https://doi.org/10.1119/10.0003900

Using mobile-device sensors to teach students error analysis
American Journal of Physics **89**, 477 (2021); https://doi.org/10.1119/10.0002906

A guide to the literature of the finite rectangular well
American Journal of Physics **89**, 529 (2021); https://doi.org/10.1119/10.0003327

AAPT 2021 PHYSICS EDUCATION®
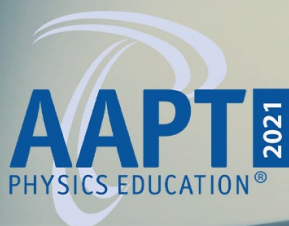
VIRTUAL SUMMER MEETING | July 31 – August 4

Magnetic diffusion, inductive shielding, and the Laplace transform

Alexander E. Krosney,[a] Michael Lang,[b] Jakob J. Weirathmueller,[c] and Christopher P. Bidinosti[d]

Department of Physics, University of Winnipeg, 515 Portage Avenue, Winnipeg, Manitoba, Canada R3B 2E9

In the quasistatic limit, a time-varying magnetic field inside a conductor is governed by the diffusion equation. Despite the occurrence of this scenario in many popular physics demonstrations, the concept of magnetic diffusion appears not to have garnered much attention itself as a subject for teaching. We employ the model of a thin conducting tube in a time-varying axial field to introduce magnetic diffusion and connect it to the related phenomenon of inductive shielding. We describe a very simple apparatus utilizing a wide-band Hall-effect sensor to measure these effects with a variety of samples. Quantitative results for diffusion time constants and shielding cutoff frequencies are consistent with a single, sample-specific parameter given by the product of the tube radius, thickness, and electrical conductivity. The Laplace transform arises naturally in regard to the time and frequency domain solutions presented here, and the utility of the technique is highlighted in several places. © *2021 Published under an exclusive license by American Association of Physics Teachers.*
https://doi.org/10.1119/10.0003508

I. INTRODUCTION

Demonstrations of the interaction between magnetic fields and non-magnetic conducting materials are very important—and popular. They provide strong, and often quite dramatic, visualizations of the Lorentz force, Faraday's law, and Lenz's law, and are typically employed to launch a discourse on the fact that electricity and magnetism, while seemingly disparate phenomena in static configurations, are truly one and the same when time variation occurs. Particular manifestations of such interactions, such as eddy currents or magnetic braking, are discussed to varying degrees in standard textbooks,[1–3] while much greater variety and detail can be found in the literature.[4–18]

To motivate our work on the related but seemingly lesser-known topic of magnetic diffusion, we begin by writing the differential equation for a time-varying magnetic field in a non-magnetic conductor (see, for example, Sec. 9.4.1 of Ref. [1])

$$\mathbf{V}^2 \boldsymbol{B}(\boldsymbol{r},t) = \mu_0 \sigma \frac{\partial \boldsymbol{B}(\boldsymbol{r},t)}{\partial t} + \mu_0 \epsilon \frac{\partial^2 \boldsymbol{B}(\boldsymbol{r},t)}{\partial t^2}, \tag{1}$$

where μ_0 is the permeability of free space, and σ and ϵ are the electrical conductivity and permittivity of the conductor, respectively. In the limit of slowly varying fields, indicative of the scenarios in the many papers mentioned above, the second-order time derivative associated with the displacement current is negligible. As a result, in this quasistatic limit, Eq. (1) is safely replaced with

$$\mathbf{V}^2 \boldsymbol{B}(\boldsymbol{r},t) = \mu_0 \sigma \frac{\partial \boldsymbol{B}(\boldsymbol{r},t)}{\partial t}, \tag{2}$$

which is indeed a form of the diffusion equation,[3,19–21] though it is rarely noted as such and few of the phenomena it describes are ever regarded as diffusive processes.

In light of this circumstance, one is tempted to re-interpret some such phenomena in terms of *magnetic diffusion*. For example, an ac magnetic field impinging on a metallic enclosure can be viewed as having insufficient time each half-cycle to fully diffuse into the conductive structure before it must start to diffuse out again. Such an effect is exacerbated with higher frequencies, thicker walls, and larger conductivities, all of which lead to increased inductive shielding. This point of view also leads one to anticipate a phase lag between the applied field and the field that has managed to *diffuse* into the enclosure. While this interpretation is certainly consistent with the physics at hand, one must concede that it is not as satisfactory as a more intuitive, standard description in terms of induced (eddy) currents and Lenz's law, say. Moreover, for the steady-state sinusoidal case, with $\boldsymbol{B}(\boldsymbol{r},t) = \boldsymbol{B}(\boldsymbol{r})e^{-i\omega t}$, the right hand side of Eq. (2) is readily replaced with $-2i\boldsymbol{B}(\boldsymbol{r})/\delta^2$ (where $\delta = \sqrt{2/\mu_0 \sigma \omega}$ is the electromagnetic skin depth[1–3]), which only further obscures the form and function of the diffusion equation. It appears then that despite the generality and ubiquity of Eq. (2), the concept of magnetic diffusion can indeed be easily overlooked.

One scenario where the notion of a magnetic field diffusing through a conductor is quite natural and intuitive is the step response.[3,19–21] Here, a switched magnetic field that would be established (near) instantaneously in the absence of the conductor now takes time to diffuse through the bulk of the material as induced eddy currents within it decay. This approach is well established in the research literature,[22–27] but is largely unknown as a teaching demonstration, as far as we can tell. In this paper, we present a simple experiment that employs a wide-band Hall-effect sensor to directly monitor the process of magnetic diffusion and determine associated time constants. The same apparatus is used without modification to make ac measurements as a function of frequency and quantify the onset of inductive shielding. The two phenomena are linked, of course, and we also take this opportunity to highlight the utility of the Laplace transform for analyzing the response of the system in both the time and frequency domains.

This paper is organized as follows. First, we develop the model of the thin conducting tube in a time-varying axial field, providing both the step and steady-state sinusoidal response and linking the two via the Laplace transform. This model is intuitive, informative, and easy to realize experimentally. Next, we describe the apparatus and experimental procedure that we employ at our institution as an undergraduate laboratory exercise. We then present and discuss results

for magnetic diffusion through conducting slabs and tubes, as well as inductive shielding of the latter. In the appendices, we provide known solutions for the general case of a conducting tube of arbitrary thickness, and also present the design method and characterization of the coil we built to generate a highly homogeneous magnetic field over the length of the tube samples.

II. THE THIN CONDUCTING TUBE IN A TIME VARYING AXIAL FIELD

Following the approach of Haus and Melcher,[19] we consider a long, cylindrical, non-magnetic tube with inner radius a, outer radius b, thickness $h \equiv b - a$, permeability μ_0, and conductivity σ, subject to an applied, uniform, axial magnetic field $B_o(t)$. Assuming the tube to be thin ($b/a \approx 1$), Ampère's law can be written as the boundary condition

$$B_i(t) - B_o(t) = \mu_0 \, h J(t), \tag{3}$$

where $B_i(t)$ is the total axial field inside the tube, $J(t)$ is an azimuthal (eddy) current density that is uniform over the thickness of the tube, and the quantity $hJ(t)$ is the instantaneous surface current that leads to the discontinuity of the field inside and outside the tube. This is, of course, just the model of an infinitely long solenoid, which produces an axial field of magnitude $\mu_0 \, h J(t)$ inside its volume and zero field outside. (Indeed, one could approach this entire problem as a long, thin, single-turn inductor of length ℓ, resistance $R = 2\pi a/\sigma h\ell$, and inductance $L = \mu_0 \pi a^2/\ell$, as done by Íñiguez *et al.*[9]) The assumption that the current density is uniform also implies that the tube is electromagnetically thin, i.e., $h \ll \delta$.

From Faraday's law of induction, we also have

$$\mathcal{E} = -\frac{d\Phi}{dt}, \tag{4}$$

where $\mathcal{E} = E(t) \, 2\pi a$ is the electromotive force associated with the induced electric field $E(t)$ driving eddy currents around the tube, and $\Phi = B_i(t) \, \pi a^2$ is the magnetic flux through the tube. Using Ohm's law $J = \sigma E$, Eq. (4) can be written as

$$\frac{2\pi a}{\sigma} J(t) = -\pi a^2 \frac{d}{dt} B_i(t). \tag{5}$$

Combining Eqs. (3) and (5) and rearranging leads to the differential equation

$$\frac{dB_i(t)}{dt} + \frac{B_i(t)}{\tau} = \frac{B_o(t)}{\tau}, \tag{6}$$

with time constant

$$\tau = \frac{1}{2} \mu_0 \sigma a h, \tag{7}$$

containing the sample-specific parameter ($\sigma a h$). Equation (6) is completely general and can be used to determine the total magnetic field inside a thin conducting tube for any uniform applied field $B_o(t)$, as is done below for a step field and a sinusoidal field. Corresponding solutions for the general case of a tube of any thickness are presented in Appendix A.

For the step field $B_o(t) = B_o$ for $t \geq 0$, the solution for initial condition $B_i(0) = 0$ is easily found to be[19,20]

$$B_i(t) = B_o \left(1 - e^{-t/\tau} \right). \tag{8}$$

The magnitude of the current density in the tube is therefore

$$J(t) = \frac{B_o}{\mu_0 h} e^{-t/\tau}. \tag{9}$$

Equations (8) and (9) show that the application of a dc step field leads, by Lenz's law, to an induced field that opposes B_o. The overall interpretation is that the applied field diffuses into the tube with the same characteristic time as the decay of the induced current. Since τ depends not only on the tube dimensions but also its composition, materials with high conductivity, such as copper, will produce long-lasting induced currents (i.e., slow diffusion of B_o), whereas a poor conductor will produce short-lived induced currents (i.e., fast diffusion of B_o.)

We now consider an ac field of the form $B_o(t) = B_o \, e^{-i\omega t}$, with frequency-independent magnitude B_o. For the steady-state sinusoidal response, one anticipates a solution of the form $B_i(t) = B_i(\omega)e^{-i\omega t}$. By substituting $B_o(t)$ and $B_i(t)$ into Eq. (6), one finds the complex amplitude[8,9,17,22]

$$B_i(\omega) = \frac{B_o}{1 - i\omega\tau}, \tag{10}$$

which reduces to $B_i(\omega) \approx B_o(1 + i\omega\tau)$ at low frequency[9,10] and goes to zero at high frequency. From this result, the induced magnetic field generated by $J(t)$ is easily determined

$$B_i(t) - B_o(t) = B_o(t) \frac{i\omega\tau}{1 - i\omega\tau}. \tag{11}$$

As expected, it is 90° out of phase with the applied field and tends to zero as $\omega \to 0$ (i.e., $\omega L \ll R$, poor shielding), while it is 180° out of phase with the applied field and approaches $-B_o(t)$ as $\omega \to \infty$ (i.e., $\omega L \gg R$, complete shielding).

The relative magnitude of the net internal field can be written as

$$\frac{|B_i(\omega)|}{B_o} = \frac{1}{\sqrt{1 + (\omega\tau)^2}} \tag{12}$$

$$= \frac{1}{\sqrt{1 + (ah/\delta^2)^2}}, \tag{13}$$

and the onset of inductive shielding is seen to occur at a cut-off frequency

$$f_c \equiv (2\pi\tau)^{-1} \tag{14}$$

$$= (\pi\mu_0\sigma a h)^{-1}, \tag{15}$$

which can also be cast as a critical thickness

$$h_c \equiv \delta^2/a \tag{16}$$

$$= (\pi\mu_0\sigma a f)^{-1}. \tag{17}$$

The latter result, noted by Fahy *et al.*,[8] often comes as a surprise: It says that the onset of shielding for this geometry occurs not when the skin depth is comparable to the thickness of the tube ($\delta \sim h$)—a commonly held misconception—but when $\delta^2 \sim ah$.[8,28] As a result, an electromagnetically thin tube with $h \ll \delta$ can still provide efficient shielding if $a \gg \delta$.

We end here by re-deriving the above results via the Laplace transform approach. In doing so, our intention is not to provide an overview of such methods—which are well described in many standard textbooks[29–32] and are further discussed in the pedagogical literature[33,34]—but rather to take the opportunity to highlight this elegant mathematical tool in the context of a very interesting and simple electromagnetic system. We will also use the Laplace transform in two other instances in this paper, making use of standard transform-pair lookup tables throughout.[29–32]

The Laplace transform of Eq. (6) with initial condition $B_i(0) = 0$ is

$$sB_i(s) + \frac{B_i(s)}{\tau} = \frac{B_o(s)}{\tau}, \tag{18}$$

where $B(s)$ denotes the transform of a magnetic field $B(t)$, and s is a complex frequency in general. Solving for $B_i(s)$ gives the Laplace transform of $B_i(t)$

$$B_i(s) = \frac{B_o(s)}{1 + s\tau}. \tag{19}$$

For the dc step field turned on at $t = 0$, $B_o(s) = B_o/s$ and Eq. (19) becomes

$$B_i(s) = \frac{B_o}{s + s^2\tau}, \tag{20}$$

which has inverse transform $B_i(t) = B_o\left(1 - e^{-t/\tau}\right)$, identical to Eq. (8).

The steady-state sinusoidal response, on the other hand, is given by $B_i(t) = H(s)B_o\,e^{-i\omega t}$ with transfer function $H(s) \equiv B_i(s)/B_o(s)$ found from Eq. (19) and evaluated at $s = -i\omega$.[31] This gives

$$B_i(t) = \left(\frac{B_o}{1 - i\omega\tau}\right)e^{-i\omega t}, \tag{21}$$

where the term in braces is the complex amplitude of Eq. (10). It is also worth noting that the transfer function found here is identical to that of a low-pass filter, which is expected intuitively for inductive shielding (i.e., low frequencies pass through the tube, high frequencies do not) and also given that an equivalent LR circuit model can be used to analyze this system.[9]

III. EXPERIMENTAL METHOD

We now describe the apparatus and experimental procedure that we use in an undergraduate laboratory exercise to make quantitative studies of magnetic diffusion and inductive shielding in conducting tubes based on the preceding theoretical model. We also present an ancillary experiment using conducting slabs that provides a very simple and intuitive demonstration of

magnetic diffusion. The two experimental configurations are shown in Fig. 1.

The specific details of the various measurements, as well as the dimensions and properties of the different samples, are presented further below. In general, however, the experimental procedure is quite simple. An electromagnetic coil, described in detail in Appendix B, is driven by a waveform generator (Rigol DG1032Z) to generate the applied magnetic field. Field measurements are made by a Hall-effect sensor (Sentron CSA-1VG)[35] with its differential output connected to two separate channels of an oscilloscope (Agilent DSO-X 2014A). The internal math function of the oscilloscope is used to determine the difference of the two channels, providing a final signal that is proportional to the magnetic field at the location of the sensor. Signal averaging using the built-in functionality of the oscilloscope is also employed. The addition of a differential amplifier between the sensor and oscilloscope could further improve performance,[28,36] but was purposely omitted here in order to keep the apparatus as simple as possible and hopefully further encourage the adoption of magnetic diffusion and ac shielding studies in the undergraduate teaching lab. The 100-kHz bandwidth of the sensor[35,36] is suitable for the time and frequency scales explored here.

A. Step field measurements

Step field measurements were performed by driving the coil with a 50-Hz square-wave voltage alternating between zero and 7.5 V. The input couplings of the oscilloscope were set to dc, and 256 averages were used. Because the analog output channel of the Hall-effect sensor is referenced to its
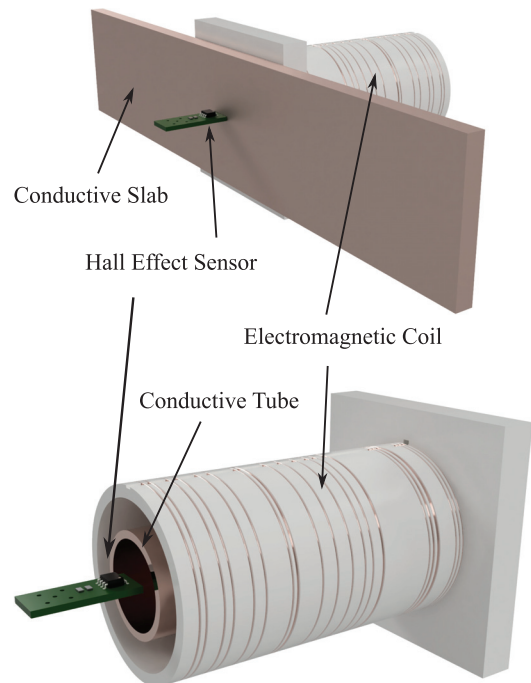

Fig. 1. Cutaway models of the two experimental configurations. The 3D-printed coil former (white) was made as a single piece with grooves for wire windings, and square end supports that act as a stand. Top: the conductive slab is placed between the Hall-effect sensor and one end of the coil. Bottom: the sensor is placed at the center of the coil and conductive tube. Both the sensor and tube are held in position by additional 3D-printed parts, which are not shown.

common output channel held at 2.5 V (giving a full scale differential output of ± 2.5 V),[35] the gain of both scope channels was set to 500 mV/div. An offset of 2.5 V was applied to both channels, and the sensitivity of the math waveform was set to 10 mV to capture the much smaller differential signal. The time constant of our coil is calculated to be 2.2 μs ($L = 129\,\mu$H, $R = 8.13\,\Omega + 50\,\Omega$ from the Rigol DG1032Z output), which is less than both the scan time ($\sim 3\,\mu$s) and rise time ($\sim 3\,\mu$s) of the sensor[35,36] and does not limit the overall bandwidth of the system. The signal of a step field measurement performed at the center of the coil in the absence of any conducting sample is shown in Fig. 2.

Given the finite bandwidth of the Hall-effect sensor, its output signal $S(t)$ must also be determined by the differential equation for a low-pass filter

$$\frac{dS(t)}{dt} + \frac{S(t)}{\tau_f} = \frac{kB(t)}{\tau_f}, \tag{22}$$

where $B(t)$ is the magnetic field at the location of the sensor, τ_f is the time constant (or rise time) of the sensor, and k is its sensitivity (~ 280 V/T for the CSA-1VG).[35] For a magnetic field of the form of Eq. (8), one can solve Eq. (22) directly by standard methods for linear first-order equations.[29,30] Conversely, one can solve by Laplace transform. By analogy with Eqs. (6) and (18), and by making use of Eq. (20) for the Laplace transform of the field of Eq. (8), one quickly finds the Laplace transform of $S(t)$

$$S(s) = \frac{1}{1 + s\tau_f} \frac{S_o}{s + s^2\tau}, \tag{23}$$

where $S_o = kB_o$. The general solution for the sensor output, along with two particularly useful limits, is thus
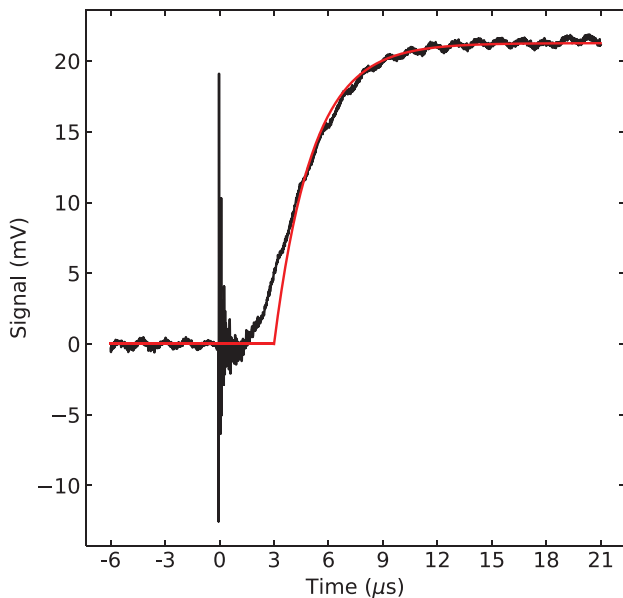

Fig. 2. The differential signal from the oscilloscope for a step field measurement using the configuration shown in the bottom of Fig. 1 with no tube. The smooth curve is an exponential fit to the data assuming an offset of exactly 3 μs to account for the sensor scan time. The fit yields a time constant of 2.1 μs, consistent with the quoted rise time of the sensor and previous tests (Refs. 35 and 36).

$$S(t) = S_o \left(1 - \frac{\tau_f e^{-t/\tau_f} - \tau e^{-t/\tau}}{\tau_f - \tau} \right), \tag{24}$$

$$= S_o \left(1 - \frac{t + \tau}{\tau} e^{-t/\tau} \right) \quad \text{when} \quad \tau_f = \tau, \tag{25}$$

$$\rightarrow S_o (1 - e^{-t/\tau}) \quad \text{when} \quad \tau_f \ll \tau. \tag{26}$$

One can also derive Eq. (24) from the Laplace convolution of $S_o \left(1 - e^{-t/\tau}\right)$ with the impulse response of the low pass filter $(1/\tau_f)e^{-t/\tau_f}$.[29–32]

Given that the magnetic diffusion time constants measured in this work are around two orders of magnitude larger than the rise time of the Hall-effect sensor ($\tau_f \sim 3\,\mu$s), Eq. (26) is appropriate here. As a result, we use as a fit function

$$S(t) = S_o(1 - e^{-(t-t_s)/\tau}), \tag{27}$$

where $t_s = 3\,\mu$s is the scan time of the sensor, and time t is measured with respect to the function generator trigger corresponding to the rising edge of the square-wave drive voltage. If thinner tubes (i.e., shorter τ) or narrower-band sensors (i.e., longer τ_f) are employed, one may need to use Eq. (24) instead. Finally, we note that given the very similar time constants of our coil and sensor, the exponential fit in Fig. 2 could be replaced by something akin to Eq. (25). This has little bearing on our present study, however, and a more detailed analysis is unwarranted here.

B. Ac field measurements

Here, the coil is driven by a 15 V_{pp} sine wave at 101 logarithmically spaced frequencies over the range $f = 1$–10,000 Hz. The oscilloscope couplings and sensitivities are the same as in Sec. III A. Over this frequency range, the magnitude of the drive circuit impedance increases by only 1%; however, the phase varies by about 8°, which is not insignificant. To account for these changes, as well as any potential frequency dependence in the receive chain, we also recorded the phase of the differential signal (relative to the trigger) and repeat the same set of frequency measurements with and without the conducting tubes. The latter represents a background measurement that is used to correct the tube data with respect to the phase and magnitude of the applied field at each frequency. A similar process has been described elsewhere.[13] Custom PYTHON code was written to automatically pass frequencies to the waveform generator and return amplitude and phase measurements from the oscilloscope. Signal averaging is set to 16 for the lowest frequencies and is dynamically increased via the program for higher-frequency measurements with tubes, which otherwise would suffer from reduced signal-to-noise ratio (SNR) due to greater inductive shielding. Overall, this strategy helps minimize run time. From Eqs. (13) and (14), data for the corrected signal amplitude are fit to the following function to extract the cutoff frequency f_c:

$$|S(f)| = \frac{S_o}{\sqrt{1 + (f/f_c)^2}}. \tag{28}$$

C. Samples

The response to a step field applied perpendicular to the face of a slab was measured for three samples—one each of

Table I. Measured properties of the tube samples. The numbers in parentheses are the uncertainty in the last digit(s) of each quantity, as determined by standard techniques (Ref. 37). The tubes are seamless, and we assume their electrical properties to be isotropic. A dc current of 5.000(5) A was used for all resistivity measurements.

Tube	h (mm)	b (mm)	ℓ (mm)	V (μV)	ρ ($10^{-8}\,\Omega\cdot$ m)	σ (10^{7} S/m)
Copper #1	0.804(7)	6.357(9)	153.0(5)	422(2)	1.66(3)	6.02(11)
Aluminum	1.468(5)	12.706(4)	153.5(5)	313(3)	4.50(5)	2.22(2)
Copper #2	1.672(15)	9.507(6)	152.0(5)	144.4(7)	1.73(2)	5.78(6)

copper, brass, and plastic. The nominal dimensions of the slabs—which were in fact borrowed from our own sliding magnet demo—are 10 in. long, 2 in. wide, and 1/4 in. thick. The response to both step and ac fields applied along the axis of a tube was measured for three samples—two of copper and one of aluminum—each nominally 6 in. long, but with different diameters and thicknesses. The precise dimensions

and measured conductivities of the tubes, which are needed for a quantitative analysis of magnetic diffusion and inductive shielding via the models in Sec. II, are given in Table I. The length ℓ, outer diameter $2b$, and thickness h of the tubes were measured with digital calipers at five different positions each to account for non-uniformities. The resistivity ρ of the samples was determined via a standard 4-wire measurement by driving a known current I through the tubes and measuring the voltage drop V across them with a digital multimeter (Agilent 34411A). From $V = IR$ and $R = \rho\ell/A$, where A is the cross-sectional area of the tube and $a = b - h$ is its inner radius, one finds

$$\frac{1}{\sigma} \equiv \rho = \frac{V}{I}\frac{\pi(b^2 - a^2)}{\ell} = \frac{V}{I}\frac{\pi(2bh - h^2)}{\ell}. \qquad (29)$$

IV. RESULTS AND DISCUSSION

A. Magnetic diffusion through slabs and tubes

The results for the slabs are shown in Fig. 3. The SNR is poor for these measurements largely due to the much weaker applied field at the location of the sensor in this configuration (see Figs. 1 and 8.) This could be improved by using a small, flat coil of many turns placed directly on the face of the slab. Still, the results presented here clearly demonstrate that, as expected, magnetic diffusion through copper is slower than it is through brass, since the former is the better conductor. Also, the step field is seen to pass through the non-conducting plastic slab near-instantaneously (i.e., indistinguishable from the rise time in Fig. 2). Another result worth noting in Fig. 3 is the near-instantaneous jump seen in the field for copper and brass, when the sensor is placed directly behind the slab but not on the center line (or axis) of the coil. By symmetry, it is only at the central location where the net field is expected to be uniquely zero just after the coil is turned on. At any other location, the induced field does not
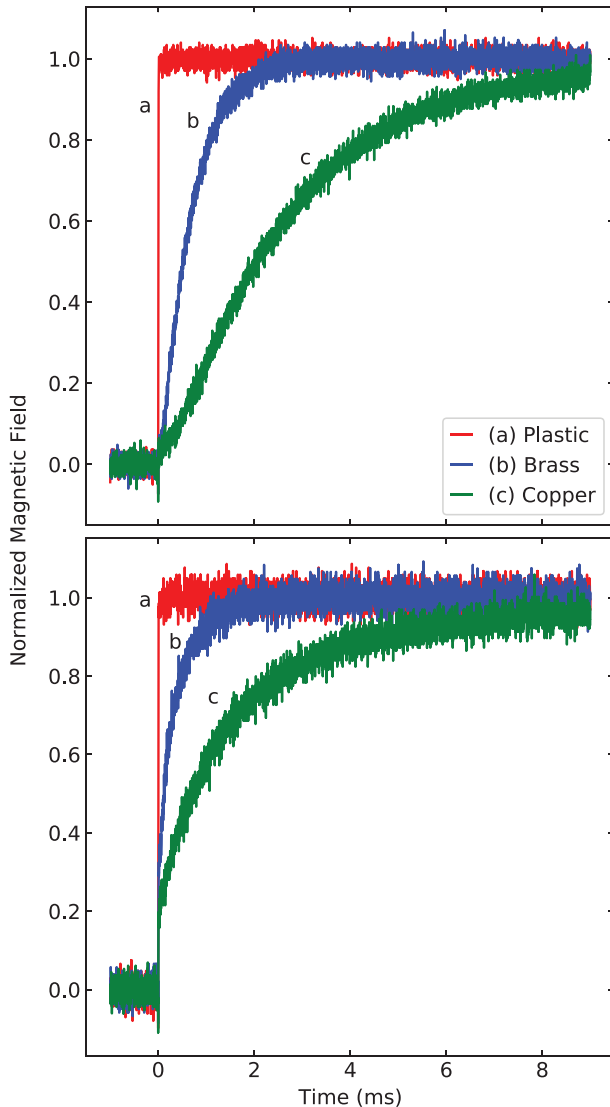

Fig. 3. The magnetic field measured at the face of the slabs opposite to the coil. The legend refers to both graphs. Top: results for a measurement position that is on the center line of the coil. Bottom: results for a measurement position that is 2.5 mm away from the center line toward the top of the slab.
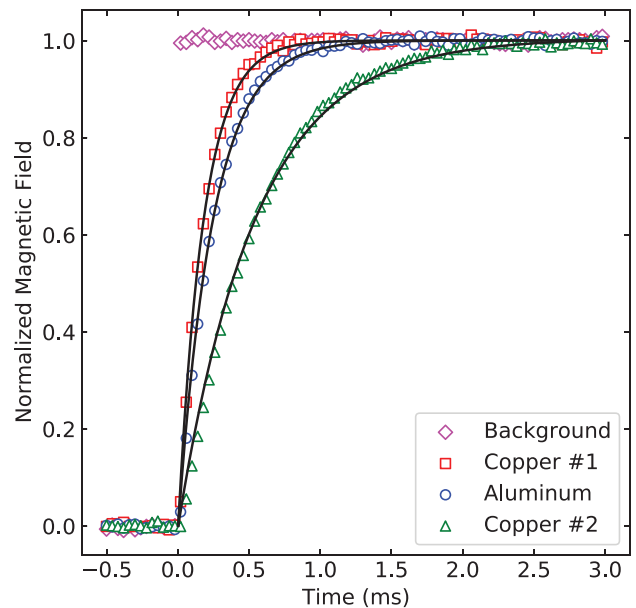

Fig. 4. The magnetic field measured at the center of the tubes. For clarity, only every 50th data point is shown. The solid lines are least-square fits to Eq. (27) for all data at $t \geq t_s = 3\,\mu$s.

Table II. Ratios of tube radii; the time constants predicted from the thin-tube model using the values given in Table I; the measured time constants extracted from fits to the data in Fig. 4; and the cutoff frequencies calculated from τ_{fit} via Eq. (14).

Tube	a/b	τ_{thin} (μs)	τ_{fit} (μs)	f_c (Hz)
Copper #1	0.874(2)	169(4)	179.3(2)	887.8(7)
Aluminum	0.8845(6)	230(3)	244.9(2)	649.9(5)
Copper #2	0.824(2)	476(7)	544.5(6)	292.3(3)

necessarily cancel the applied field. Equivalently, one can think of this result as being a consequence of the magnetic field lines initially wrapping around the exterior of the slab while its interior is still fully shielded by the induced currents. Again, because of symmetry, there can be no magnetic field at the central point located directly on the back (or front) face of the slab, since the approaching field lines must spread out in opposite directions about this point.

The results for the tubes are shown in Fig. 4 along with a background measurement (i.e., no tube) for comparison. Time constants are determined from fits to Eq. (27) with $t_s = 3 \mu s$ and are compiled in Table II along with predicted values from the thin-tube model. Our results largely agree with the rule-of-thumb that the thin-tube model should be good to within ∼10% for $a/b \geq 2/3$.[20,25] The greatest discrepancy is seen with our thickest sample, which perhaps suggests that one should use tubes with a/b closer to 0.9, say, if the goal is to provide teaching demonstrations that agree very closely with the thin-tube model. We also point out that time constants predicted from the general model (Eq. (A6)) are closer to, but still do not agree within error, with our measured values. Still, these results provide an excellent demonstration of magnetic diffusion, consistent with the trends predicted from measured sample properties. With a good degree of confidence, then, we use our values of τ_{fit} here to predict the cutoff frequencies for the ac measurements of Sec. IV B. These are also listed in Table II.

B. Inductive shielding by tubes

Example data of the ac signals measured at the center of the tubes are shown in Fig. 5 for a drive frequency of 1 kHz. At this frequency, all samples exhibit a clear phase shift with respect to the voltage trigger, as well as a reduction in amplitude with respect to the background value. These are both hallmarks of the presence of eddy currents and thus the onset of inductive shielding. (Indeed, it is very informative for students to simply observe how the signal on the oscilloscope changes for a given sample as they increase the drive frequency on the function generator.) From the comparative results shown in Fig. 5, it is also clear that the degree of shielding for the different tubes is consistent with their respective cutoff frequencies predicted from the diffusion measurements above (Table II) or by what one would estimate from their properties in Table I via Eq. (15).

It is also possible to discern a small phase shift in the background signal in Fig. 5. This is due to the complex
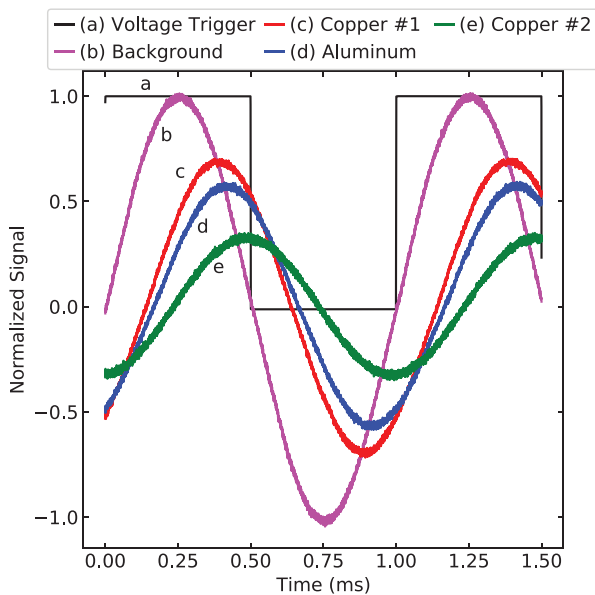

Fig. 5. Signal waveforms at a drive frequency of 1 kHz. Amplitudes are normalized with respect to the background value (21.9 mV) measured here.
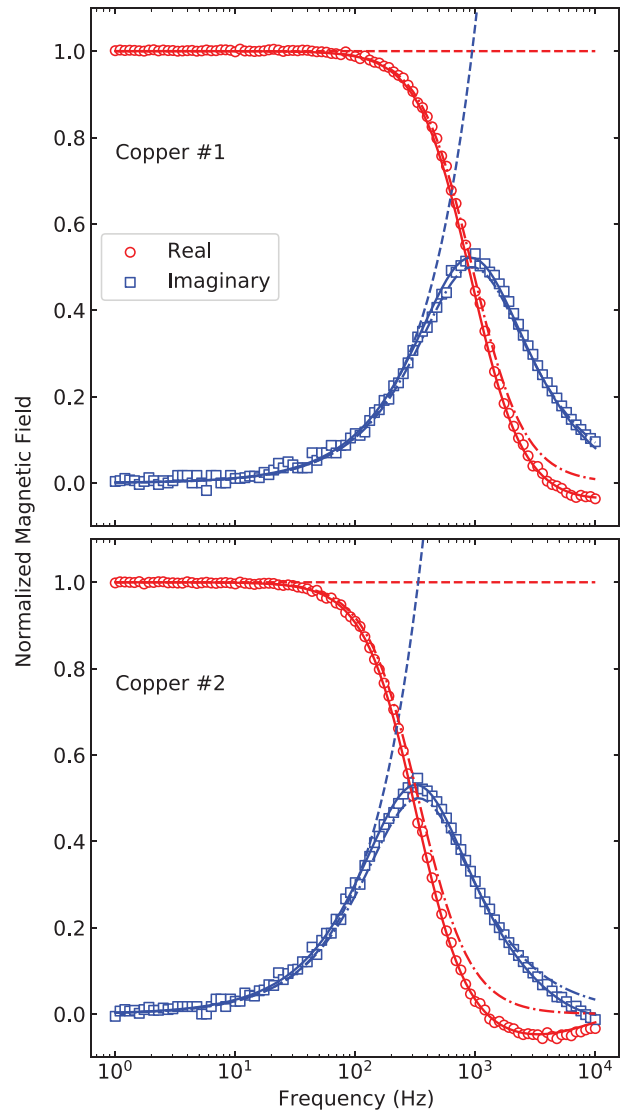

Fig. 6. Complex components of the internal magnetic field for the copper tubes. The legend refers to both graphs. The solid and dashed-dotted lines are the functional form for the general model (Eq. (A7)) and the thin-tube model (Eqs. (13) and (7)), respectively. The dashed lines are the low-frequency limit (Refs. 9 and 10) of the latter as discussed in Sec. II.

impedance of the drive circuit arising from the inductance of the coil. To correctly extract the complex components of the field inside the tubes, the raw data of the type shown in Fig. 5 must be corrected with respect to the phase and amplitude of the background signal at each frequency as discussed in Sec. III B. The results of this process are shown in Fig. 6 for the two copper samples. Overlaid on top of these data are curves for the general model (Appendix A), the thin-tube model, and the low-frequency limit of the latter generated using the sample properties given in Table I. The low-frequency model proposed by Íñiguez et al.[9,10] is suitable to a few hundred hertz or less for these samples, while the thin-tube model can extend the range of study by perhaps another order of magnitude. The general model, on the other hand, provides excellent agreement over the full frequency range studied here. The limitation of the thin-tube model is easily understood from the well-known rule-of-thumb that the skin depth of copper is roughly 1 cm at 60 Hz, which translates to 3 mm at 670 Hz or 1 mm at 6 kHz. Looking at the copper tube thicknesses given in Table I, then, one sees that the condition of being electromagnetically thin (i.e., $h \ll \delta$) will certainly break down over the frequency range studied here, and deviations from the thin-tube model are to be expected at the higher frequencies.

To better highlight the inductive shielding of the tubes, as well as their behavior as low-pass filters, the magnitude of the internal field is plotted versus frequency in Fig. 7 for all tube samples. The low-frequency end of the data are fit to Eq. (28), and cutoff frequencies are compiled in Table III along with predicted values from the thin-tube model. We chose to limit the fitting range to data with normalized amplitude greater than 0.5, which from Fig. 6 still show good agreement with the thin-tube model. The predicted cutoff frequencies from Table II are also presented in Fig. 7 and show good agreement with the ac measurements. A final feature of interest in Fig. 7 is the slight decrease in amplitude

Table III. Cutoff frequencies predicted for the thin-tube model using the values given in Table I; the measured cutoff frequencies extracted from fits to the data in Fig. 7; and the ratios h/δ and ah/δ^2 calculated from $f_{c,\text{fit}}$.

Tube	$f_{c,\text{thin}}$ (Hz)	$f_{c,\text{fit}}$ (Hz)	h/δ	ah/δ^2
Copper #1	942(20)	946(2)	0.381(8)	1.00(4)
Aluminum	691(8)	710(1)	0.366(4)	1.03(2)
Copper #2	335(5)	327(1)	0.457(7)	0.98(2)

seen in the background measurement at high frequencies. This again is due to the small increase in coil impedance; all sample data have been corrected for this by normalizing to the background amplitude at each frequency value as mentioned above. With regard to the results in Table III, one can see that all measured values of cutoff frequency agree to within a few percent or less with the values predicted from the thin-tube model. Also, as shown in the last two columns of the table, the onset of inductive shielding does indeed occur when $\delta^2 \sim ah$ and not when $\delta \sim h$.[8,28]

V. CONCLUSION

A review of the literature reveals that the concept of magnetic diffusion is rarely considered for the purposes of pedagogy.[38] The thin conducting tube in a uniform, time-varying axial field provides a complete and very accessible model for exploring magnetic diffusion as well as the related phenomenon of inductive shielding. The product of the tube radius, thickness, and electrical conductivity provides a single, sample-specific parameter that sets both the time constant for stepped dc fields to diffuse through the tube and the cutoff frequency for ac fields to penetrate the interior of the tube. While not required, the use of the Laplace transform to solve for and link the time and frequency domain solutions of this system further broadens the educational experience here.

A simple apparatus utilizing a wide-band Hall-effect sensor allows either stepped or ac measurements without any configurational changes. The addition of a differential amplifier following the Hall-effect sensor could further improve performance. As it stands, the present setup provides more than sufficient SNR to make meaningful qualitative and quantitative tests on a variety of samples. Time constants and cutoff frequencies extracted from the two types of measurement for conducting tubes show good agreement with each other as well as with predicted values.

Through a judicious choice of frequency range and tube thickness, one can design a student laboratory experiment that resides fully within the limits of the thin-tube model ($h \ll a, \delta$). This could be desirable from the point of view of minimizing the amount of information needed to understand the experiment. Still, many students will likely wonder what happens as the skin depth becomes smaller than the tube thickness, say. The general solutions (also provided here) answer such questions and should be well within reach for an advanced undergraduate student.
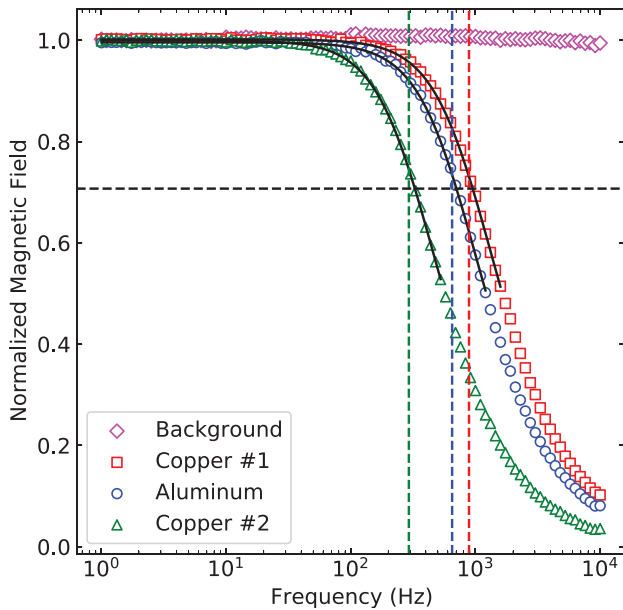

Fig. 7. Normalized magnitude of the internal field as a function of frequency. The solid lines are least-square fits of Eq. (28) to all data points with ordinate value greater than 0.5. The horizontal dashed line indicates the half-power amplitude $1/\sqrt{2}$ that defines the cutoff frequency of a low-pass filter. The vertical dashed lines indicate the cutoff frequency predicted for each tube from the preceding step field measurements (see Table II).

APPENDIX A: SOLUTIONS FOR THE CONDUCTING TUBE OF ARBITRARY THICKNESS

For the general problem of a uniform, axial field $\boldsymbol{B}_o(t) = B_o(t)\hat{z}$ applied to a non-magnetic, conducting tube of any thickness, one must solve the diffusion equation in the bulk of the tube, subject to boundary conditions. For this geometry, Eq. (2) becomes

$$\frac{\partial^2 B_z(\rho,t)}{\partial \rho^2} + \frac{1}{\rho}\frac{\partial B_z(\rho,t)}{\partial \rho} = \mu_0\sigma\frac{\partial B_z(\rho,t)}{\partial t}. \tag{A1}$$

Solutions are provided below; derivations are found in the accompanying references.

For a step field $B_o(t) = B_o$ for $t \geq 0$, the solution for the internal field subject to initial condition $B_i(0) = 0$ can be written as[20,21,23]

$$B_i(t) = B_o\left(1 - \sum_{n=1}^{\infty} c_n e^{-t/\tau_n}\right), \tag{A2}$$

with coefficients

$$c_n = \frac{4}{a^2}\frac{J_0(b\gamma_n)J_2(a\gamma_n)}{\gamma_n^2(J_0^2(b\gamma_n) - J_2^2(a\gamma_n))} \tag{A3}$$

and time constants

$$\tau_n = \frac{\mu_0\sigma}{\gamma_n^2}, \tag{A4}$$

where γ_n is the n-th root of the equation

$$J_0(b\gamma)Y_2(a\gamma) - Y_0(b\gamma)J_2(a\gamma) = 0, \tag{A5}$$

and J_ν and Y_ν are Bessel functions of the first and second kind of order ν. After sufficient time has passed $(t > \mu_0\sigma/\gamma_1^2)$, the field within the conductor volume can described by the $n=1$ term only. In this case, the field is once again given by Eq. (8) with time constant[20]

$$\tau = \frac{\mu_0\sigma}{\gamma_1^2}. \tag{A6}$$

For an ac field $B_o(t) = B_o e^{-i\omega t}$, the solution for the complex amplitude of the internal field is[8,22]

$$B_i(\omega) = B_o\frac{2}{z_i^2}[I_0(z_o)K_2(z_i) - K_0(z_o)I_2(z_i)]^{-1}, \tag{A7}$$

where $z_i = (1-i)a/\delta$, $z_o = (1-i)b/\delta$, and I_ν and K_ν are modified Bessel functions of the first and second kind of order ν. One can show that this is equivalent to the result given by Íñiguez et al.,[11] keeping in mind that the latter employs $e^{i\omega t}$ for the temporal dependence of the applied field, which leads to a conjugate solution.

Finally, based on the discussion in Sec. II, the Laplace transform of $B_i(t)$ for the step response divided by the Laplace transform of the step function $(1/s)$ should lead to the complex amplitude $B_i(\omega)$ for the steady-state sinusoidal response. The procedure is trivial here and starting from Eq. (A2) one quickly arrives at

$$B_i(s) = B_o\left(1 - s\sum_{n=1}^{\infty}\frac{c_n\tau_n}{1 + \tau_n s}\right), \tag{A8}$$

which evaluated at $s = -i\omega$ gives an alternative form of Eq. (A7). We have shown the two solutions to be numerically equivalent for the tube parameters and frequency range studied here. We did not attempt to prove mathematical equivalence, although it appears the necessary details can be gleaned from the work of Jaeger.[23]

The solutions presented in this appendix are also valid for a non-magnetic, conducting tube in a uniform, transverse magnetic field.[22,23] As a result, they also hold for a uniform field applied at any angle to the axis of the tube. This is not the case for the more general scenario of a magnetic tube, however.[21–23]

APPENDIX B: NUMERICAL OPTIMIZATION OF THE DRIVE COIL FOR IMPROVED HOMOGENEITY

We originally built a standard solenoid comprising two layers of 100 evenly spaced windings to serve as a drive coil. The solenoid was wound with #32 AWG enameled magnet wire on a 3D-printed former. We found the time constant of this coil was greater than that of the Hall-effect sensor (see Fig. 2), so we decided to re-make it with the same dimensions and wire but using only 50 windings per layer. We also took this opportunity to optimize the winding pattern to provide greater field homogeneity over the length of the tube samples. While this does offer greater fidelity with our theoretical models, it is not critical for obtaining satisfactory results, and preliminary tests with our original solenoid did yield nearly identical time constants and cutoff frequencies to those reported above.

The details of the optimization algorithm are given below. The final winding pattern and 3D former can be seen in Fig. 1. The specific locations of the current loops are given in Table IV, allowing one to easily duplicate our coil or scale it to any desired radius. The calculated magnetic field profiles of the optimized coil and the original solenoid are shown in Fig. 8, along with those of the well-known Lee-Whiting and Helmholtz designs[39] for comparison. The parameters of the various coils are summarized in Table V. For the Lee-Whiting and Helmholtz coils, we considered two designs: fixing either their length or their radius to equal those of our solenoid and optimized coil. Measurements of the field profile along the axis of the optimized coil are also shown in Fig. 8 and confirm the expected improvement in homogeneity. Accurate measurements of the off-axis field are more challenging to achieve and were

Table IV. The axial positions of the current loops comprising the optimized coil in ascending order by column. The values, normalized to the coil radius R and rounded to the third decimal point, give the distance z_i to the i-th loop on either side of the central plane of the coil $(z=0)$. For our coil $R = 2.28$ cm, which is the average radius for the two layers of #32 AWG wire (thickness 0.2 mm).

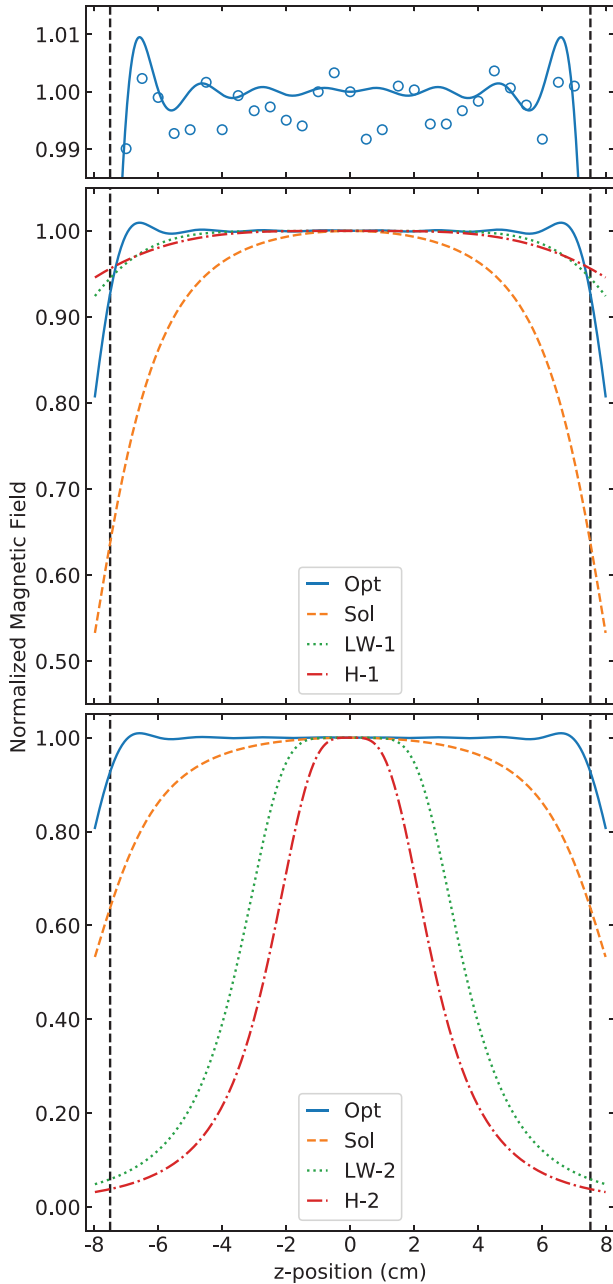| $\pm z_i/R$				
0.163	0.887	1.744	2.350	3.129
0.234	1.195	1.933	2.997	3.140
0.426	1.250	2.098	3.052	3.396
0.525	1.261	2.201	3.063	3.451
0.745	1.555	2.339	3.118	3.505

Fig. 8. Calculated profiles of $B_z(0, z)$ for the various coils listed in Table V. The vertical dashed lines indicate the optimization region of $z = \pm 7.5$ cm. Measurements of the optimized coil made with the Hall-effect sensor (circles, top panel) confirm a field homogeneity within 1% over almost the full length of the tubes used here. The Lee-Whiting and Helmholtz coils would require a large radius (middle panel) to achieve a comparable homogeneity.

not pursued here. However, for an axisymmetric coil such as this, the constraint of Maxwell's equations ensures that the homogeneity of the field away from the central axis must similarly improve.[40]

Our design optimization was performed by considering the net axial field produced by the sum of contributions from the symmetric pairs of current loops[1–3] comprising the coil

$$B(z) = \sum_i^{N/2} \frac{\mu_0 R^2 I/2}{\left(R^2 + (z - z_i)^2\right)^{3/2}} + \frac{\mu_0 R^2 I/2}{\left(R^2 + (z + z_i)^2\right)^{3/2}},$$

(B1)

Table V. Coil parameters for the optimized (Opt), solenoid (Sol), Lee-Whiting (LW), and Helmholtz (H) coils. The coil efficiency χ is defined here as the calculated central field strength $B_z(0, 0)$ per unit current divided by the total number of turns N comprising each coil type. The coil radius R is taken to be the average of the two layers for the Opt and Sol designs; while all turns are assumed to exist on the same radius for the LW and H designs. The half-length L is the axial location of the outermost current loop for all designs.

Coil	χ (μT/A/turn)	N	R (cm)	L (cm)
Opt	6.55	100	2.28	7.98
Sol	7.51	200	2.28	7.98
LW-1	4.07	26	8.48	7.98
H-1	2.82	2	15.95	7.98
LW-2	15.18	26	2.28	2.14
H-2	19.76	2	2.28	1.14

where z_i is the distance to the i-th loop on either side of the central plane of the coil, and the current I was set to unity. To begin, all loops are evenly spaced as per a regular solenoid. Optimizing the axial field homogeneity over a distance z_{opt} requires minimizing the integral

$$\int_0^{z_{opt}} \left| \frac{B(z) - B(0)}{B(0)} \right| dz.$$

(B2)

This was done by randomly selecting a pair of symmetric loops and displacing them a distance δz away from and towards $z = 0$. If either displacement reduces Eq. (B2), the changes are saved and another pair is randomly selected; otherwise, the changes are discarded. Random selection continues until further displacement of all pairs does not result in an improvement, in which case the value of δz is decreased. Once δz is reduced beyond a set minimum threshold value (typically given by the resolution of the 3D printer), the program exits and saves the final z_i values.

To prevent overlap and wire grooves with a separation wall smaller than printing capabilities, additional constraints are placed on the current loop locations. If moving a pair places their wires within a minimum threshold distance relative to another pair, two calculations are performed. The first bundles the neighboring wires such that they form adjacent windings within a single groove. Alternatively, the wires are spaced exactly by the minimum threshold value. If either scenario improves field homogeneity, the changes are saved; otherwise, they are discarded.

a)Electronic mail: krosney-a83@webmail.uwinnipeg.ca

b)Electronic mail: mlang.physics@gmail.com

c)Electronic mail: weirathj@myumanitoba.ca; Present address: Max Rady College of Medicine, University of Manitoba, 750 Bannatyne Avenue, Winnipeg, Manitoba, Canada R3E 0W2.

d)Author to whom correspondence should be addressed. Electronic mail: c.bidinosti@uwinnipeg.ca

[1] D. J. Griffiths, *Introduction to Electrodynamics*, 4th ed. (Pearson, Boston, 2013).

[2] G. L. Pollock and D. R. Stump, *Electromagnetism* (Addison Wesley, San Francisco, 2002).

[3] A. Garg, *Classical Electromagnetism in a Nutshell* (Princeton U. P., Princeton, 2012).

[4] W. M. Saslow, "Maxwell's theory of eddy currents in thin conducting sheets, and applications to electromagnetic shielding and MAGLEV," Am. J. Phys. **60**, 693–711 (1992).

[5] M. A. Nurge et al., "Drag and lift forces between a rotating conductive sphere and a cylindrical magnet," Am. J. Phys. **86**, 443–452 (2018).

[6]M. H. Partovi and E. J. Morris, "Electrodynamics of a magnet moving through a conducting pipe," Can. J. Phys. **84**, 253–271 (2006).

[7]B. Irvine et al., "Magnet traveling through a conducting pipe: A variation on the analytical approach," Am. J. Phys. **82**, 273–279 (2014).

[8]S. Fahy et al., "Electromagnetic screening by metals," Am. J. Phys. **56**, 989–992 (1988).

[9]J. Íñiguez et al., "Measurement of the electrical conductivity of metallic tubes by studying magnetic screening at low frequency," Am. J. Phys. **73**, 206–210 (2005).

[10]J. Íñiguez et al., "Measurement of electrical conductivity in nonferromagnetic tubes and rods at low frequencies," Am. J. Phys. **77**, 949–953 (2009).

[11]J. Íñiguez et al., "The electromagnetic field in conductive slabs and cylinders submitted to a harmonic longitudinal magnetic field," Am. J. Phys. **77**, 1074–1081 (2009).

[12]C. P. Bidinosti et al., "The sphere in a uniform rf field—Revisited," Concepts Magn. Resonance **31B**, 191–202 (2007).

[13]M. L. Honke and C. P. Bidinosti, "The metallic sphere in a uniform ac magnetic field: A simple and precise experiment for exploring eddy currents and non-destructive testing," Am. J. Phys. **86**, 430–438 (2018).

[14]J. R. Nagel, "Induced eddy currents in simple conductive geometries: mathematical formalism describes the excitation of electrical eddy currents in a time-varying magnetic field," IEEE Antennas Propag. Mag. **60**(1), 81–88 (2018). See also "Correction," IEEE Antennas Propag. Mag. **60**(4), 83 (2018).

[15]P. J. H. Tjossem and E. C. Brost, "Optimizing Thomson's jumping ring," Am. J. Phys. **79**, 353–358 (2011).

[16]C. L. Ladera and G. Donoso, "Unveiling the physics of the Thomson jumping ring," Am. J. Phys. **83**, 341–348 (2015).

[17]R. W. Latham and K. S. H. Lee, "Theory of inductive shielding," Can. J. Phys. **46**, 1745–1752 (1968).

[18]J. R. Reitz, "Forces on moving magnets due to eddy currents," J. Appl. Phys. **41**, 2067–2071 (1970).

[19]H. A. Haus and J. R. Melcher, *Electromagnetic Fields and Energy* (Prentice-Hall, Englewood Cliffs, 1989), Chap. 10.

[20]H. E. Knoepfel, *Magnetic Fields: A Comprehensive Theoretical Treatise for Practical Use* (John Wiley & Sons, New York, 2000), Chap. 4.

[21]W. R. Smythe, *Static and Dynamic Electricity*, 2nd ed. (McGraw-Hill, New York, 1950), Chap. XI.

[22]L. V. King, "XXI. Electromagnetic shielding at radio frequencies," London, Edinburgh, Dublin Philos. Mag. J. Sci. **15**(97), 201–223 (1933).

[23]J. C. Jaeger, "III. Magnetic screening by hollow circular cylinders," London, Edinburgh, Dublin Philos. Mag. J. Sci. **29**(192), 18–31 (1940).

[24]C. P. Bean et al., "Eddy-current method for measuring the resistivity of metals," J. Appl. Phys. **30**, 1976–1980 (1959).

[25]M. A. Weinstein, "Magnetic decay in a hollow circular cylinder," J. Appl. Phys. **33**, 762 (1962).

[26]K. Lee and G. Bedrosian, "Diffusive electromagnetic penetration into metallic-enclosures," IEEE Trans. Antennas Propag. **27**, 194–198 (1979).

[27]M. J. Ramos et al., "The phase angle method for electrical resistivity applied to the hollow circular cylinder geometry," J. Appl. Phys. **67**, 1167–1169 (1990).

[28]C. P. Bidinosti and M. E. Hayden, "Selective passive shielding and the Faraday bracelet," Appl. Phys. Lett. **93**, 174102 (2008).

[29]M. L. Boas, *Mathematical Methods in the Physical Sciences*, 3rd ed. (John Wiley & Sons, Hoboken, 2006), Chap. 8.

[30]K. F. Riley, M. P. Hobson, and S. J. Bence, *Mathematical Methods for Physics and Engineering*, 3rd ed. (Cambridge U. P., Cambridge, 2006), Chap. 13.

[31]C. A. Desoer and E. S. Kuh, *Basic Circuit Theory* (Mcgraw-Hill, New York, 1969), Chap. 13.

[32]I. S. Gradshteyn and I. M. Ryzhik, *Table of Integrals, Series, and Products*, 7th ed. (Elsevier, Amsterdam, 2007), Chap. 17.

[33]K. Riess, "Some applications of the Laplace transform," Am. J. Phys. **15**, 45–48 (1947).

[34]C. L. Bohn and R. W. Flynn, "Real variable inversion of Laplace transforms: An application in plasma physics," Am. J. Phys. **46**, 1250–1254 (1978).

[35]See datasheet and application notes—in particular, *Current Sensing with the CSA-1V*—at the distributor website <https://gmw.com/product/csa-1vg-so/>. The CSA-1V comes in a standard, surface mount SOIC-8 package, for which small breakout PCBs can be purchased from many vendors.

[36]C. P. Bidinosti et al., "A simple wide-band gradiometer for operation in very low background field," Concepts Magn. Resonance **37B**, 1–6 (2010).

[37]J. R. Taylor, *An Introduction to Error Analysis: The Study of Uncertainties in Physical Measurements*, 2nd ed. (University Science Books, Sausalito, 1996), Chaps. 3 and 4.

[38]See supplementary material at https://www.scitation.org/doi/suppl/10.1119/10.0003508 for a more extensive list of papers on the interaction of magnetic fields and conducting materials.

[39]J. L. Kirschvink, "Uniform magnetic fields and double-wrapped coil systems: Improved techniques for the design of bioelectromagnetic experiments," Bioelectromagnetics **13**, 401–411 (1992).

[40]S. R. Muniz and V. S. Bagnato, "Analysis of off-axis solenoid fields using the magnetic scalar potential: An application to a Zeeman-slower for cold atoms," Am. J. Phys. **83**, 513–517 (2015).